Monthly Notices
of the
ROYAL ASTRONOMICAL SOCIETY

Mon. Not. R. Astron. Soc. **427,** 3396–3405 (2012) doi:10.1111/j.1365-2966.2012.22022.x

Broad-band timing properties of the accreting white dwarf MV Lyrae

S. Scaringi,[1]★ E. Körding,[1] P. Uttley,[2] P. J. Groot,[1] C. Knigge,[3] M. Still[4,5] and P. Jonker[1,6,7]

[1]*Department of Astrophysics/IMAPP, Radboud University Nijmegen, PO Box 9010, 6500 GL Nijmegen, the Netherlands*
[2]*Astronomical Institute 'Anton Pannekoek', University of Amsterdam, Science Park 904, 1098 XH Amsterdam, the Netherlands*
[3]*Department of Physics and Astronomy, University of Southampton, Highfield, Southampton SO17 1BJ*
[4]*NASA Ames Research Center, Moffett Field, CA 94035, USA*
[5]*Bay Area Environmental Research Institute, Inc., 560 Third St. West, Sonoma, CA 95476, USA*
[6]*SRON, Netherlands Institute for Space Research, Sorbonnelaan 2, 3584 CA Utrecht, the Netherlands*
[7]*Harvard-Smithsonian Center for Astrophysics, 60 Garden Street, Cambridge, MA 02138, USA*

Accepted 2012 August 29. Received 2012 August 29; in original form 2012 July 3

ABSTRACT

We present a broad-band timing analysis of the accreting white dwarf system MV Lyrae based on data obtained with the *Kepler* satellite. The observations span 633 d at a cadence of 58.8 s and allow us to probe four orders of magnitude in temporal frequency. The modelling of the observed broad-band noise components is based on the superposition of multiple Lorentzian components, similar to the empirical modelling adopted for X-ray binary systems. We also present the detection of a frequency varying Lorentzian component in the light curve of MV Lyrae, where the Lorentzian characteristic frequency is inversely correlated with the mean source flux. Because in the literature similar broad-band noise components have been associated with either the viscous or dynamical time-scale for different source types (accreting black holes or neutron stars), we here systematically explore both scenarios and place constraints on the accretion disc structure. In the viscous case we employ the fluctuating accretion disc model to infer parameters for the viscosity and disc scale height, and infer uncomfortably high parameters to be accommodated by the standard thin disc, whilst in the dynamical case we infer a large accretion disc truncation radius of $\approx 10 R_{\rm WD}$. More importantly however, the phenomenological properties between the broad-band variability observed here and in X-ray binaries and active galactic nuclei are very similar, potentially suggesting a common origin for the broad-band variability.

Key words: accretion, accretion discs – black hole physics – binaries: close – novae, cataclysmic variables – stars: oscillations – stars: individual: MV Lyrae.

1 INTRODUCTION

Compact interacting binaries (CBs) are close binary systems usually consisting of a late-type star that transfers material on to a black hole (BH), a neutron star (NS) or a white dwarf (WD) via Roche lobe overflow. With an orbital period on the order of hours, the donor star transfers material through the L1 point, which forms an accretion disc surrounding the compact object. The dynamics and physics governing the flow of matter accreting on to the compact objects is, however, still debated. The accretion discs in BH and NS binary systems (X-ray binaries or XRBs) emit most of their radiation in X-rays, whilst the accretion discs in accreting WDs (cataclysmic variables or CVs) emit mostly in the optical/ultraviolet (UV) wavebands. This is a consequence of the gravitational potential well created by the central compact object: for CVs the innermost edge of the accretion disc sits at a few thousand gravitational radii, whilst for galactic BH and NS the inner disc reaches down to a few gravitational radii.

Most CVs and XRBs are highly variable sources in X-rays and/or optical/UV. This variability has been associated with the accretion disc from the characteristic frequencies observed in the power spectral density (PSD). For example, the presence of periodic modulations slightly longer than the orbital period can be associated with positive superhumps caused by a tidal deformation in the accretion disc (Whitehurst 1988; Osaki 1989; Lubow 1991). This has been modelled and observed in CVs (Wood et al. 2011; Montgomery 2012), as well as in XRBs (O'Donoghue & Charles 1996).

Another example of similar timing characteristics between CVs and XRBs is the presence of both dwarf nova oscillations (DNOs)

★E-mail: s.scaringi@astro.ru.nl

and quasi-periodic oscillations (QPOs). In both cases DNOs/QPOs appear in the PSD at a few tens of mHz (Warner 2004; Pretorius, Warner & Woudt 2006), whilst for XRBs they appear at few hHz, and are referred to as lower kHz oscillations (Belloni, Psaltis & van der Klis 2002). The phenomenological similarity between the QPOs and DNOs observed in CVs and XRBs was first noted by Mauche (2002) and Warner (2004), where the ratio of periods is $P_{\rm QPO}/P_{\rm DNO} \approx 15$, and holds over six orders of magnitude in temporal frequency. The physical reason for this relation is not fully understood, although some suggestions have been proposed (Belloni et al. 2002), all involving accretion disc dynamics, but none seems to be able to explain all observations consistently (Warner 2004; Pretorius et al. 2006).

In addition to periodic or quasi-periodic signals, both CVs and XRBs possess an intrinsic aperiodic broad-band noise continuum, generally described as flickering in CVs. This red noise component produces a continuum that rises towards low frequencies. In the XRB context, this is usually modelled a by simple power law (e.g. $1/f$) or by a sum of broad Lorentzian components (Belloni et al. 2002), with a characteristic break at $\approx 10^{-3}$ Hz for CVs and $\approx$1 Hz for XRBs (Belloni et al. 2002; Revnivtsev et al. 2012). This component has been shown to display a linear rms–flux relation in XRBs and active galactic nuclei (AGN; Uttley & McHardy 2001), where the root-mean-square (rms) variability linearly scales with flux over a wide range of time-scales. More recently, the same relation has been also observed in the CV system MV Lyrae, albeit at lower frequencies (Scaringi et al. 2012, hereafter Paper I). The detection of the rms–flux relation in both CVs and XRBs strongly suggests that the broad-band variability originates within the accretion disc. Under certain assumptions about the origin of the variability and the physics of the mass-transfer process, the characteristics of the broad-band noise can be used to constrain the strength of the effective viscosity that drives the mass transfer through the disc (Ingram & Done 2010, 2011).

Motivated by the similarities between the periodic and aperiodic signals in CVs and XRBs, we here study the broad-band temporal frequency spectrum of the CV MV Lyrae in search of further similarities between the two classes of objects. MV Lyrae is one of 14 known CVs in the *Kepler* field-of-view (FOV), and is classified as being a VY Scl nova-like system, spending most of its time in a high state ($V \approx$ 12–13), but occasionally (every few years) undergoing short-duration (weeks to months) drops in brightness ($V \approx$ 16–18; Hoard et al. 2004). The reason for these sudden drops in luminosity is not clear, but Livio & Pringle (1994) have suggested starspots from the donor covering the L1 point inhibiting mass transfer. It is known however that MV Lyrae has an extremely low mass transfer rate at its minimum brightness ($3 \times 10^{-13}\,{\rm M}_{\odot}\,{\rm yr}^{-1}$; Hoard et al. 2004; Linnell et al. 2005), where the WD is detected at $V \approx 18$ and dominates the emitted light. Furthermore, the orbital period of 3.19 h has been determined for the system, as well as a low inclination of $i \sim 11^{\circ}$–13° (Skillman, Patterson & Thorstensen 1995).

In Paper I we analysed the high-frequency (tens of minutes) broad-band variability for MV Lyrae with data obtained with the *Kepler* satellite. In this paper we will analyse the same light curve at lower temporal frequencies, with particular emphasis on the varying broad-band components during the observation. MV Lyrae has been observed with *Kepler* during a low-to-high luminosity transition, when its optical emission originates mostly from its nearly face-on disc.

In Section 2, we briefly describe the *Kepler* data acquisition, and the procedure we use to construct broad-band PSDs. We fit the PSDs with a combination of Lorentzian shaped functions to characterize the observed broad-band noise components. Section 3 shows our results, with particular emphasis on one frequency-varying broad-band noise component, which appears to correlate with the mean source flux. Finally, in Section 4, we consider whether the inferred broad-band noise components can be associated with fluctuations on either the dynamical or viscous time-scales in the accretion disc. As we shall see, both of these interpretations lead to uncomfortable implications for the accretion disc structure.

2 DATA ANALYSIS

The MV Lyrae light curve[1] was provided to us by the Science Operations Centre in reduced and calibrated form after being run through the standard data reduction pipeline (Jenkins et al. 2010). Similarly to Paper I, we only consider the single aperture photometry (SAP) light curve. Data gaps occasionally occur due to *Kepler* entering anomalous safe modes (see the *Kepler Data Characteristics Handbook*).[2] Here, we make no attempt to correct these artefacts, but simply remove them from the light curve. Fig. 1 shows the short cadence (58.8 s; Gilliland et al. 2010), barycentre-corrected, light curve for MV Lyrae obtained during the first eight quarters of *Kepler* operations. The light curve spans an interval of 633 d. The visible data gaps present in the light curve are due to the artefacts described in Paper I as well as the monthly data down-links.

In order to obtain the time-averaged PSDs, we have split the light curve in Fig. 1 into 120 non-overlapping segments, each covering 5.275 d. This time-scale has been chosen to probe the lowest frequencies without being affected by low-frequency power generated by the long-term trends in flux during the observation (see Fig. 1). We computed the fast Fourier transform (FFT) of 118 segments, ignoring two segments due to the large data gap at $\approx$750 d in Fig. 1. We further applied the rms normalization of Miyamoto et al. (1991) so that the square root of the integrated PSD power over a specific frequency range yields the rms variability. After computing the normalized PSDs for each segment we obtain the intrinsic spread in each frequency bin by computing the standard deviation of the 118 PSDs, shown in Fig. 2.

At first glance we note large scatter in the time-averaged PSD, caused by the varying PSD shape and normalization during the 633-d observation. Furthermore, many incoherent features are clear from Fig. 2. Specifically, we see a clear broad Lorentzian-shaped feature peaking at about 10^{-3} Hz, briefly discussed in Paper I, but also excess power at about 10^{-4} and 10^{-5} Hz. It is hard to determine whether the excess power is caused by a single intrinsically broad feature or a blend of many. In order to shed light on which of these interpretations is correct we have produced a dynamic FFT of the light curve. This is shown in Fig. 3, where we have again computed rms-normalized PSDs on 5.275-d segments, but this time with a 50 per cent overlap, for clarity. The apparent gaps are caused by data gaps in the light curve shown in Fig. 1. Fig. 3 suggests that the excess power between $10^{-3.5}$ and 10^{-4} Hz is produced by a single, frequency-varying QPO whose peak frequency is initially near $10^{-3.5}$ Hz and then slowly declines on a time-scale of $\approx$250 d. A comparison with the light curve in Fig. 1 also suggests a possible correlation between the peak frequency of this QPO and the mean flux of the system. We will return to this correlation in Section 3.

[1] The *Kepler* response function for the photometry covers the wavelength range 4000–9000 Å.

[2] http://archive.stsci.edu/kepler/documents.html

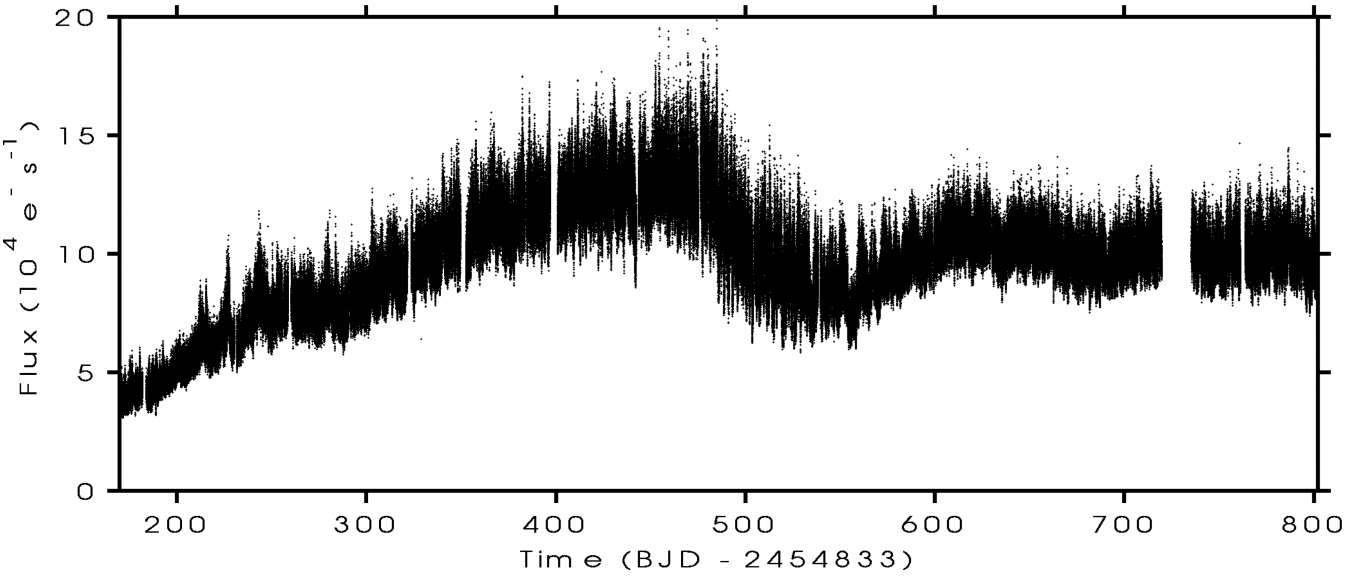

Figure 1. MV Lyrae light curve obtained by the *Kepler* satellite in short cadence mode (58.8 s).

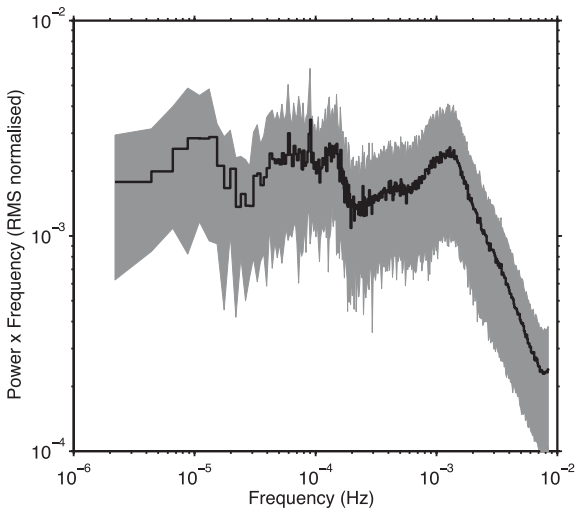

Figure 2. Time-averaged PSD of MV Lyrae. The shaded region shows the 1σ width of the distribution spanned by the 118 single 5.275 d PSDs, whilst the thick line shows their average.

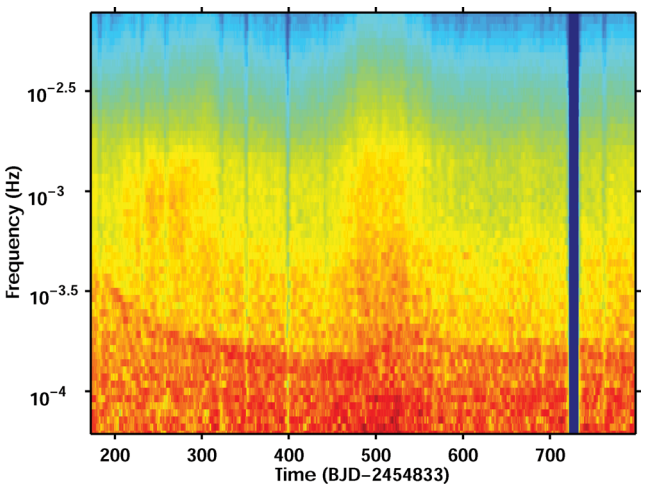

Figure 3. Rms-normalized dynamic PSD of the MV Lyrae light curve shown in Fig. 1. Each PSD has been computed on a 5.275-d segment, with a 50 per cent overlap.

2.1 PSD fitting

In order to quantify and fit the frequency-varying QPO(s), we first produced 118 rms-normalized PSDs, each from 5.275 d, non-overlapping data segments. Next, we averaged five consecutive PSDs (except in one case where we averaged three due to a large data gap in the light curve) and binned these into ≈550 equally spaced frequency intervals. The bin size is somewhat arbitrary, but has been chosen as a compromise to increase the signal-to-noise ratio in each bin while retaining a high frequency resolution. We further obtained the intrinsic scatter in each frequency bin by calculating the standard deviation of the five PSDs used. This intrinsic scatter is larger than the statistical errors, and we thus adopt the intrinsic scatter as a conservative estimate of the errors of each frequency bin, which also takes into account fluctuations in the intrinsic PSD shape. This procedure resulted in 24 time-averaged PSDs.

The fit to each PSD was carried out by starting with a simple broken power-law fit to which we added successive Lorentzian component until the reduced χ^2 was near unity. The shape of the Lorentzians was taken from Belloni et al. (2002):

$$P(\nu) = \frac{r^2\Delta}{\pi}\frac{1}{\Delta^2 + (\nu - \nu_0)^2}, \quad (1)$$

where r is the integrated fractional rms and Δ is the half-width at half-maximum. With this definition the Lorentzians attain their maximum power in $\nu P(\nu)$ at the characteristic frequency:

$$\nu_{\rm max} = \frac{1}{t_{\rm max}} = \sqrt{\nu_0^2 + \Delta^2}. \quad (2)$$

The broken power law takes the form

$$P(\nu) = \frac{A\nu^{-1}}{1 + \frac{\nu}{\nu_{\rm br}}}, \quad (3)$$

where A is the normalization and $\nu_{\rm br}$ the break frequency. With this definition the PSD shape has a slope of -1 up to $\nu_{\rm br}$, where the slope then changes to -2, similarly to the PSDs observed in some AGN and XRBs (Summons et al. 2007). In our analysis we are

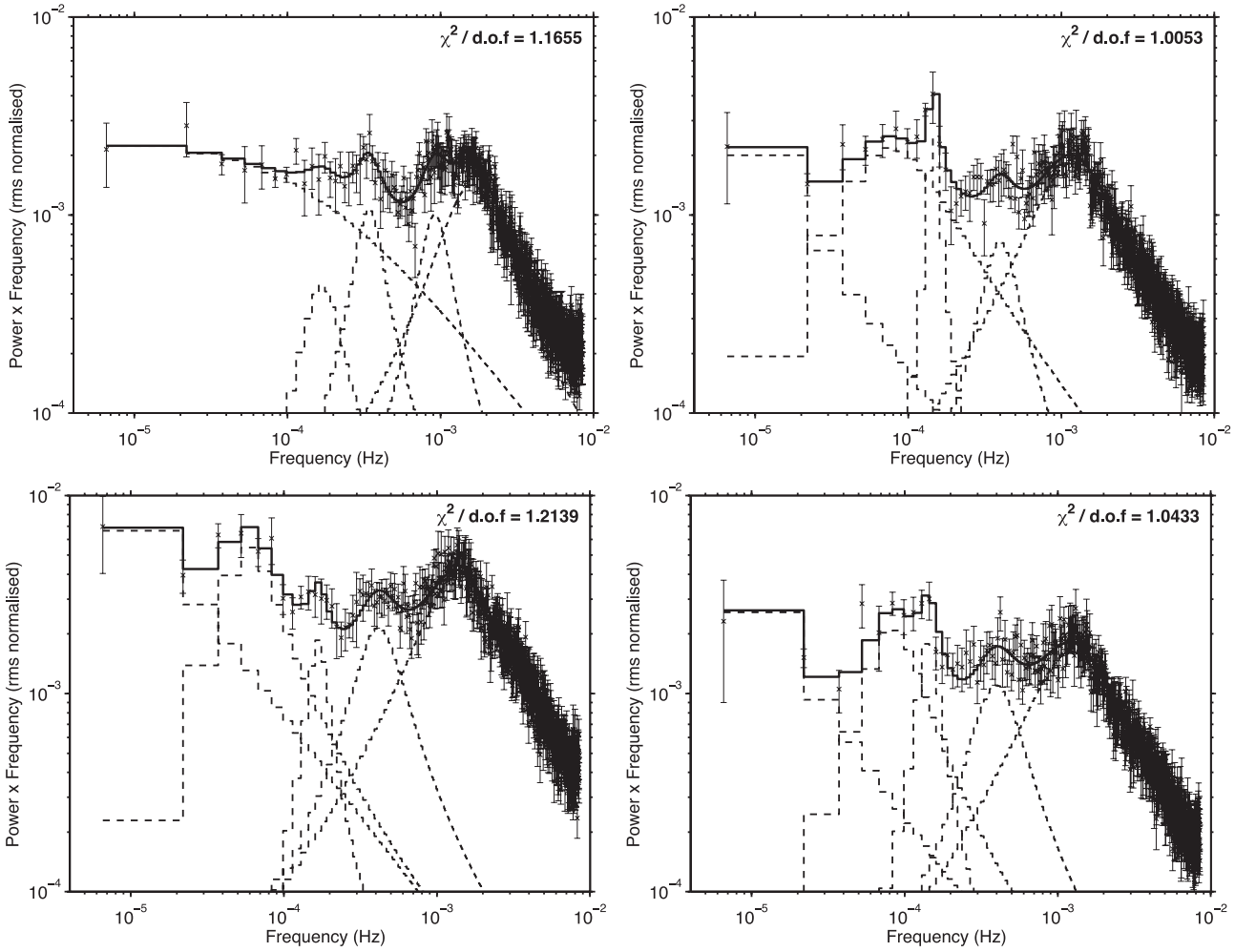

Figure 4. PSDs in νP_ν form for MV Lyrae, also showing the best-fitting model components. The PSDs have been created by averaging 5 5.275 d PSDs. From top-left to bottom-right the central observation times are, respectively, 182.7, 367.3, 525.5, 789.1 in BJD 245 4833.

mainly interested in the properties of the fitted Lorentzian, and use the low-frequency power-law model to account for any systematic excess power generated by the long-term trends (such as the steady flux increase) observed in the light curve shown in Fig. 1.

3 RESULTS

We fit each of the 24 PSDs individually, taking into account the Poisson noise level. We find that all PSDs require four Lorentzians. Of course, this does not exclude the possibility that more components could be present in the data, hidden beneath the noise level. Fig. 4 shows some examples of our fits, whilst Table 1 shows the resulting best-fitting parameters for all our fits, where we labelled our Lorentzians from 1 to 4 in ascending order of frequency. In a few cases when two Lorentzians were highly blended the fits resulted in some parameters being unconstrained.

We searched for possible correlations within the fit parameters and both observation time and mean source flux. In this respect, interesting trends with observation time are found within the characteristic frequencies of the Lorentzians $\nu_{\max}$, shown in Fig. 5. The most prominent correlation however is found between the characteristic frequency of Lorentzian L_3 and the mean source flux, which obtained a Spearman correlation coefficient of -0.89, and is shown in Fig. 6. To date, no similar correlation to that observed here has been reported for a CV, and we will discuss the possible origin of such variability in the next section. No other fit parameters display a clear trend with either flux or time.

The high-frequency break, modelled by the Lorentzian L_1, is seen to slightly change in frequency, but does not correlate with mean flux (see top left-hand panel of Fig. 5). However, one interesting trend within the Lorentzian L_1 arises by looking at the integrated fractional rms, r_A, as a function of time, shown in Fig. 7. The two peaks at $\approx$250 and $\approx$500 d coincide with a small plateau and a decrease in flux within the MV Lyrae light curve, respectively. Both these features, and the break frequency, will be discussed in more detail in the next section.

As mentioned in the introduction, correlations between some of the Lorentzian components are observed in XRBs and some CVs. Specifically, the two-QPO correlation diagram produced for XRBs (Belloni et al. 2002) and for CVs (Warner 2004) can be described by $P_{\rm QPO}/P_{\rm DNO} \approx 15$. We have searched for a similar correlation between the four fitted Lorentzians in MV Lyrae. In Fig. 8 we show plots for the characteristic frequencies of all four fitted Lorentzians. In order to determine whether any of these pairs is statistically correlated we performed a Monte Carlo correlation analysis similar to that used in Scaringi et al. (2010).

For each pair of characteristic frequencies we created two data sets. In the first (set A) we replaced each of the values with a

Table 1. Best-fitting parameters for the 24 time-averaged PSDs of MV Lyrae. In cases where the fit parameters were unconstrained no error bars are given.

			L_1			L_2						
Time	Mean flux	r	ν_0	Δ	r	ν_0	Δ					
(BJD 255 4833)	(10^4 e$^-$s^{-1})	(10^{-2})	(10^{-4} Hz)	(10^{-4} Hz)	(10^{-2})	(10^{-4} Hz)	(10^{-4} Hz)					
182.69	4.29	4.77 ± 0.49	13.97 ± 1.44	7.62 ± 0.61	2.79 ± 0.71	8.83 ± 0.36	2.20 ± 0.88					
209.06	5.69	5.70 ± 1.47	11.21 ± 2.43	8.06 ± 1.00	4.11 ± 2.06	7.53 ± 0.54	3.27 ± 1.75					
235.43	7.20	8.67 ± 0.39	8.23 ± 0.49	5.87 ± 0.23	1.00 ± 1.17	6.96 ± 0.60	0.69 ± 1.38					
261.79	7.70	8.48 ± 0.19	8.80 ± 0.25	5.09 ± 0.21	0.94 ± 0.32	4.80 ± 0.11	0.18 ± 0.15					
288.16	7.85	8.54 ± 0.21	9.68 ± 0.33	5.96 ± 0.20	2.64 ± 0.57	4.24 ± 0.26	1.44 ± 0.58					
314.52	9.10	7.48 ± 0.23	9.01 ± 0.59	8.09 ± 0.30	2.80 ± 0.46	4.09 ± 0.17	1.17 ± 0.35					
340.88	10.32	6.23 ± 0.34	8.43 ± 0.89	7.61 ± 0.39	2.83 ± 0.87	3.66 ± 0.39	1.54 ± 0.71					
367.25	11.41	6.20 ± 0.19	9.36 ± 0.52	7.04 ± 0.31	2.65 ± 0.42	3.73 ± 0.19	1.16 ± 0.33					
393.62	12.20	3.94 ± 0.27	10.23 ± 0.36	4.58 ± 0.52	0.99 ± 0.14	3.58 ± 0.04	0.10 ± 0.04					
419.98	12.71	5.76 ± 0.14	9.00 ± 0.42	6.99 ± 0.28	2.63 ± 0.31	3.45 ± 0.11	0.86 ± 0.19					
446.35	12.90	6.35 ± 0.22	8.52 ± 0.69	8.02 ± 0.39	2.57 ± 0.39	3.24 ± 0.16	1.00 ± 0.30					
472.72	12.92	9.12 ± 0.31	8.03 ± 0.70	8.59 ± 0.32	3.12 ± 0.66	3.68 ± 0.22	1.21 ± 0.44					
499.09	10.40	9.69 ± 0.45	10.46 ± 0.67	8.32 ± 0.31	5.75 ± 1.15	2.81 ± 0.52	2.36 ± 0.77					
525.45	9.05	8.80 ± 0.28	11.17 ± 0.57	7.83 ± 0.37	5.20 ± 0.49	3.76 ± 0.17	1.56 ± 0.30					
551.82	8.41	7.32 ± 0.22	10.94 ± 0.67	8.50 ± 0.48	2.40 ± 0.39	4.33 ± 0.15	0.75 ± 0.27					
578.19	9.40	5.39 ± 0.23	11.13 ± 0.62	7.61 ± 0.34	4.29 ± 0.39	3.57 ± 0.20	2.00 ± 0.34					
604.55	10.48	4.77 ± 0.37	11.38 ± 1.18	8.49 ± 0.56	3.96 ± 0.52	4.22 ± 0.27	2.41 ± 0.57					
630.92	10.53	5.12 ± 0.28	9.71 ± 0.94	8.96 ± 0.40	2.88 ± 0.64	3.47 ± 0.41	2.10 ± 0.73					
657.28	10.35	4.84 ± 0.20	10.81 ± 0.83	8.33 ± 0.53	2.74 ± 0.41	4.13 ± 0.18	1.19 ± 0.32					
683.65	9.71	5.12 ± 0.32	10.70 ± 1.11	8.74 ± 0.52	3.55 ± 0.60	4.20 ± 0.29	1.93 ± 0.52					
710.01	10.18	4.82 ± 0.46	8.94 ± 1.72	9.43 ± 0.65	2.61 ± 0.74	4.31 ± 0.39	2.11 ± 0.89					
736.38	9.98	5.19 ± 0.30	9.49 ± 1.15	8.94 ± 0.51	2.64 ± 0.49	4.28 ± 0.25	1.56 ± 0.52					
762.74	10.06	5.71 ± 0.29	8.86 ± 1.00	8.45 ± 0.45	2.53 ± 0.48	4.45 ± 0.19	1.20 ± 0.41					
789.11	10.02	6.10 ± 0.35	9.53 ± 1.01	7.92 ± 0.50	3.80 ± 0.58	3.58 ± 0.24	1.56 ± 0.45					
		L_3			L_4							
r	ν_0	Δ	r	ν_0	Δ	A	$\nu_{\rm br}$	χ^2(d.o.f)				
(10^{-2})	(10^{-4} Hz)	(10^{-5} Hz)	(10^{-2})	(10^{-4} Hz)	(10^{-5} Hz)	(10^{-3})	(10^{-5} Hz)					
2.81 ± 0.37	3.23 ± 0.14	7.71 ± 2.03	2.11 ± 0.87	1.53 ± 0.17	5.06 ± 3.63	2.32 ± 0.07	16.22 ± 4.46	628.22(539)				
2.33 ± 0.46	2.64 ± 0.04	2.49 ± 0.88	4.60 ± 0.86	1.42 ± 0.15	10.11 ± 3.30	2.15 ± 0.11	3.41 ± 0.76	572.12(539)				
2.04 ± 0.62	1.94 ± 0.06	2.75 ± 1.34	6.58 ± 1.32	0.48 ± 0.24	8.55 ± 2.32	10.64 ± 3.24	0.35 ± 0.17	634.09(539)				
2.35 ± 0.27	1.81 ± 0.02	1.41 ± 0.45	7.60 ± 0.79	0.22 ± 0.17	8.33 ± 1.13	5.00	0.27 ± 0.02	573.31(540)				
2.88 ± 0.16	1.63 ± 0.02	1.53 ± 0.21	2.04 ± 0.28	1.08 ± 0.02	1.13 ± 0.60	1.85 ± 0.08	7.51 ± 1.54	678.57(539)				
2.17 ± 0.19	1.58 ± 0.02	0.85 ± 0.20	9.02 ± 0.61	0.17 ± 0.08	5.55 ± 0.44	9.89 ± 0.51	0.10	491.48(540)				
2.95 ± 0.20	1.47 ± 0.01	0.87 ± 0.14	8.89 ± 2.06	0.24 ± 0.16	4.60 ± 0.47	5.39 ± 37.38	0.18 ± 1.59	620.69(539)				
2.78 ± 0.22	1.39 ± 0.01	1.10 ± 0.31	8.41 ± 0.38	0.40 ± 0.03	5.67 ± 0.54	15.15 ± 0.48	0.10	542.88(540)				
2.35 ± 0.13	1.27 ± 0.02	0.99 ± 0.14	2.76 ± 0.19	0.59 ± 0.01	1.35 ± 0.31	1.47 ± 0.03	68.14 ± 11.31	646.78(539)				
1.68 ± 1.90	1.26 ± 0.05	0.29 ± 0.99	7.48 ± 0.76	0.40 ± 0.08	5.52 ± 0.52	7.02 ± 2.73	0.46 ± 0.31	652.78(539)				
3.00 ± 0.27	1.24 ± 0.01	1.14 ± 0.30	6.34 ± 0.37	0.57 ± 0.02	3.45 ± 0.44	3.80	1.18 ± 0.09	571.55(540)				
3.84 ± 3.33	1.22 ± 0.01	0.34 ± 0.89	8.44 ± 1.31	0.43 ± 0.07	4.07 ± 0.66	5.01 ± 1.35	1.14 ± 0.92	611.36(539)				
2.48 ± 0.47	1.46 ± 0.04	1.88 ± 0.63	7.68 ± 0.36	0.55 ± 0.01	1.87 ± 0.15	11.23 ± 1.64	0.72 ± 0.21	503.37(539)				
3.17 ± 0.41	1.58 ± 0.04	2.73 ± 0.77	9.50 ± 0.59	0.45 ± 0.02	2.51 ± 0.25	15.80 ± 4.22	0.48 ± 0.22	654.27(539)				
1.99 ± 0.63	1.87 ± 0.08	2.31 ± 1.45	7.78 ± 0.93	0.60 ± 0.08	5.35 ± 0.96	7.09 ± 1.44	0.82 ± 0.37	663.23(539)				
2.41 ± 0.24	1.60 ± 0.03	2.34 ± 0.41	4.62 ± 0.27	0.64 ± 0.02	2.98 ± 0.35	3.41 ± 0.40	0.90 ± 0.23	561.41(539)				
3.27 ± 0.53	1.34 ± 0.04	2.85 ± 0.63	5.70 ± 0.89	0.54 ± 0.05	3.75 ± 0.95	1.46 ± 1.24	0.57 ± 0.94	657.11(539)				
1.92 ± 0.23	1.42 ± 0.02	1.21 ± 0.30	6.68 ± 0.32	0.55 ± 0.03	5.31 ± 0.50	1.90	0.47 ± 0.03	459.03(540)				
2.40 ± 10.08	1.39 ± 0.02	0.21 ± 2.04	9.51 ± 1.15	0.24 ± 0.12	6.18 ± 0.47	1.02 ± 6.46	0.32 ± 3.10	589.60(539)				
1.90 ± 0.59	1.32 ± 0.04	1.94 ± 0.94	7.52 ± 0.81	0.48 ± 0.06	5.35 ± 0.80	1.50 ± 0.66	0.96 ± 1.12	556.03(539)				
2.23 ± 3.48	1.38 ± 0.01	0.30 ± 1.34	5.51 ± 0.57	0.75 ± 0.03	3.32 ± 0.56	1.06 ± 0.09	5.48 ± 4.20	565.27(539)				
3.20 ± 13.70	1.54 ± 0.01	0.15 ± 1.38	8.13 ± 0.89	0.36 ± 0.07	4.22 ± 0.36	5.01 ± 16.93	0.19 ± 0.87	602.86(539)				
2.21 ± 0.34	1.41 ± 0.03	1.74 ± 0.55	8.29 ± 1.13	0.32 ± 0.11	5.30 ± 0.54	5.01 ± 17.83	0.19 ± 0.89	538.07(539)				
3.21 ± 0.63	1.34 ± 0.04	2.29 ± 0.70	5.77 ± 0.72	0.68 ± 0.03	3.55 ± 0.90	10.56 ± 6.00	0.21 ± 0.16	562.37(539)				

random variable drawn from a normal distribution whose mean is equal to the fitted characteristic frequencies and whose standard deviation is equal to the respective errors. In the second (set B) we additionally shuffled the order of one of the two frequencies, thus randomizing the correlation rank. We produced 200 000 samples for each set, and computed the correlation coefficient ρ for each. The mean values of the ρ distributions obtained from set A will then yield the *intrinsic* correlation coefficients, taking into account the errors. The corresponding set B distribution will instead yield the width of the ρ distribution in the absence of any correlation (which

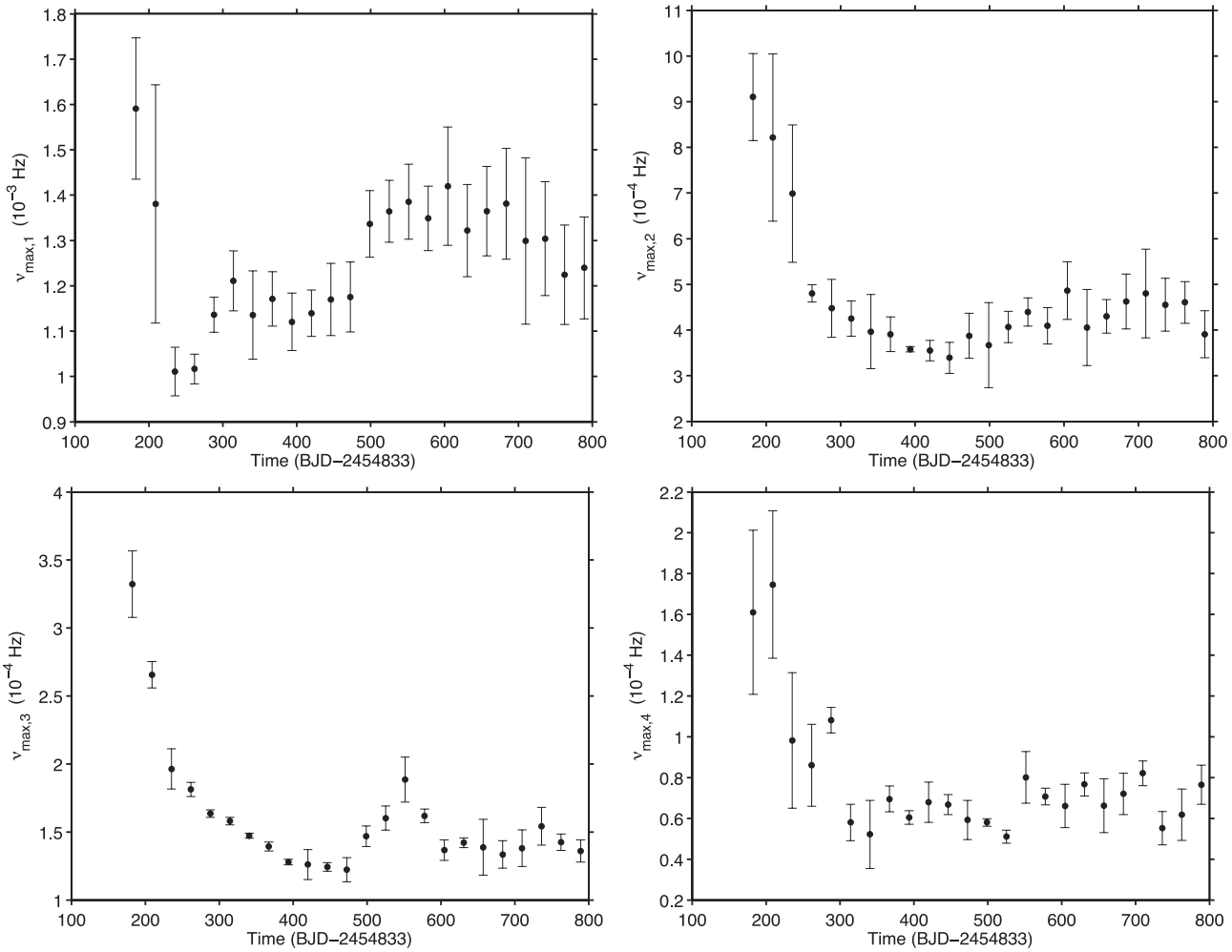

Figure 5. Characteristic frequency, ν_{max}, versus observation time for the four Lorentzians L_1, L_2, L_3 and L_4 from top-left to bottom-right, respectively.

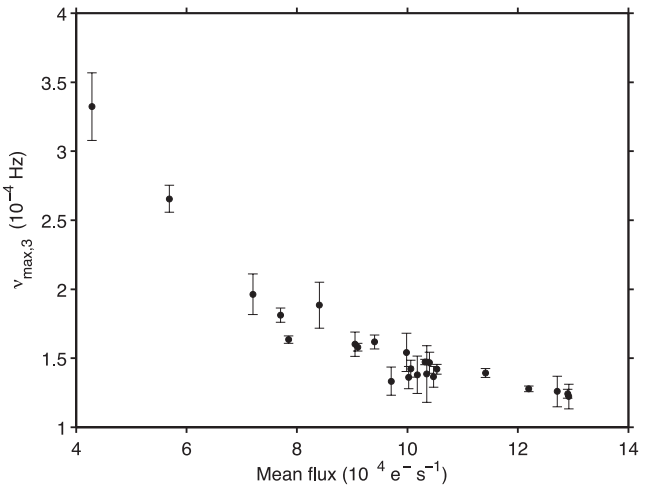

Figure 6. Correlation between the characteristic time-scale t_{max} of the Lorentzian L_3 and mean source flux.

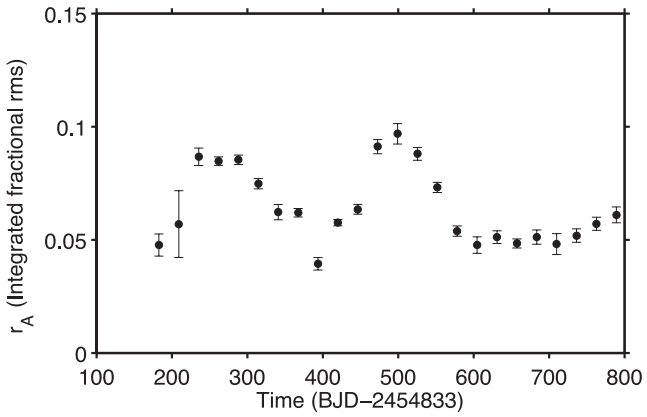

Figure 7. Evolution of the integrated fractional rms r_1 of the Lorentzian L_1 as a function of observing time.

is centred at 0). The statistical significance for each pair is then found by determining where the obtained mean ρ values from set A fall on the obtained distribution of our mock data set B. This analysis thus allows us to determine the correlation significance of the observed characteristic frequency pairs by taking into account the errors on each observation.

In Fig. 8 we show in the top right-hand panels plots for the characteristic frequency pairs, whilst in the bottom left-hand panels we show the resulting ρ distribution from our first simulation and

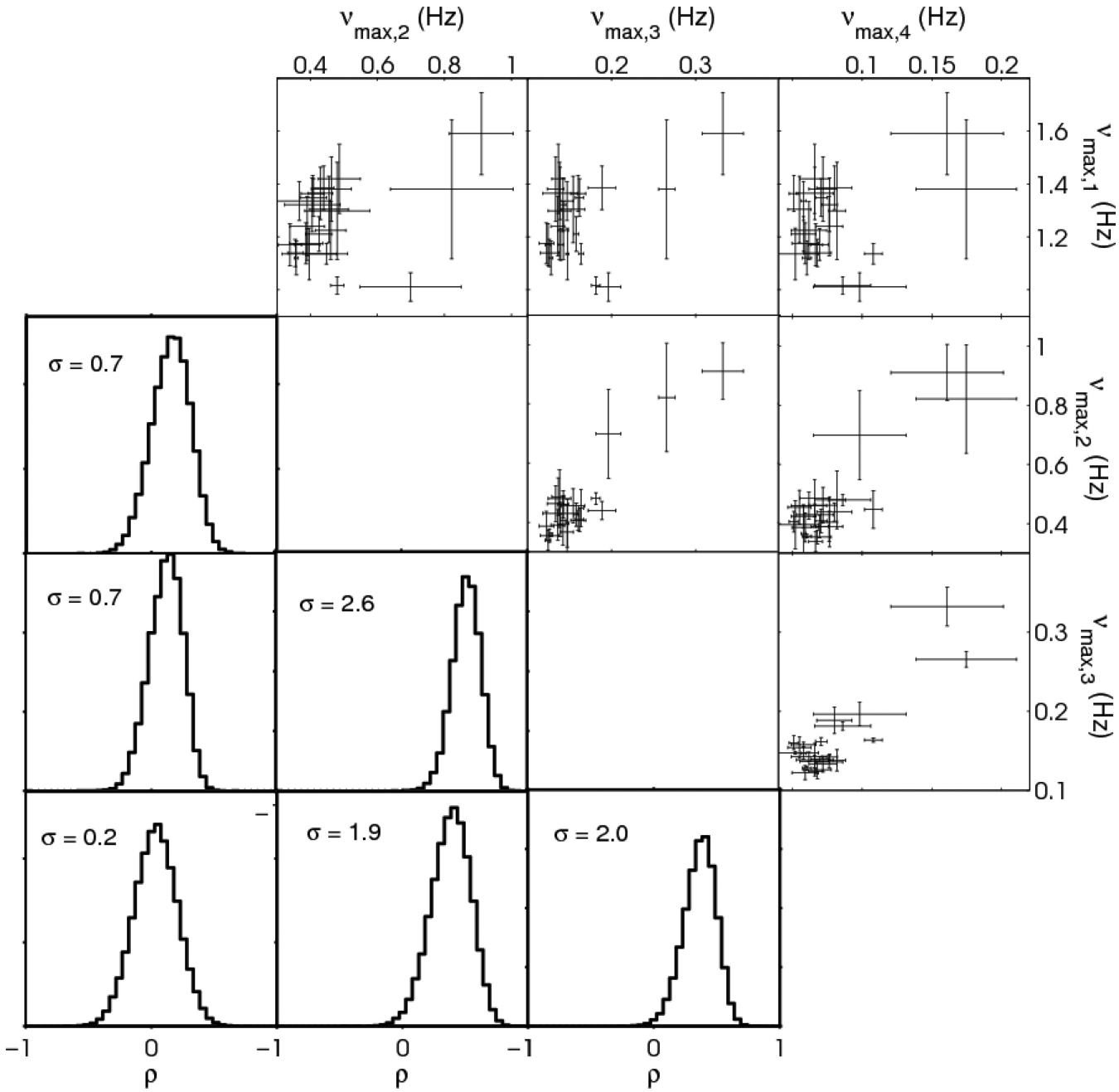

Figure 8. The top-right half of the figure shows the characteristic frequencies of the fitted Lorentzians. The bottom-left part of the figure shows the corresponding Spearman rank correlation coefficient values ρ obtained from the analysis described in Section 3 together with the corresponding correlation significance. Each panel matches its reflection along the diagonal.

the corresponding correlation significance. None of the Lorentzian pairs is observed to display a clearly statistically significant correlation. However, it is still possible that some pairs may be correlated, and the low-frequency cluster of data points is biasing our observation. For example, the pair $\nu_{\rm max,3}$ versus $\nu_{\rm max,2}$, which obtained the highest significance ($\sigma = 2.6$) in our analysis, as well as some other pairs, do suggest this. However, further measurements are required at the highest frequencies in order to determine if this is the case. If the $\nu_{\rm max,3}$ versus $\nu_{\rm max,2}$ pair were to be correlated after all, our analysis suggests they would follow the relation $t_{\rm max,3}/t_{\rm max,2} \approx 3$, different from the known $P_{\rm QPO}/P_{\rm DNO} \approx 15$ relation (Belloni et al. 2002; Warner 2004).

4 DISCUSSION

Here we discuss the implications of the observed QPO/broad-band noise component frequencies with regard to the standard, optically thick, geometrically thin accretion disc model (Shakura & Sunyaev 1973). Given the low binary inclination of $i = 11^\circ$–13° (Skillman et al. 1995), the WD magnitude seen in the faint state (Hoard et al. 2004) and the result from Paper I, we are confident that most of the emitted light observed in the *Kepler* passband is originating from the accretion disc. In what follows we will always assume $M_{\rm WD} = 0.722\,{\rm M}_\odot$ (Hoard et al. 2004), and a WD radius of $\approx 7 \times 10^8$ cm.

The observed characteristic frequencies are usually associated with the dynamical or viscous time-scale (Uttley & McHardy 2001; Ingram & Done 2010, 2011; Revnivtsev et al. 2012). While it is not yet clear if one of these two time-scales is the correct one, most other time-scales of interest (such as thermal) lie between these two. We will thus discuss them as likely limiting cases. The dynamical time-scale is given by

$$\nu_{\rm dyn}(r) = \frac{1}{t_{\rm dyn}(r)} = \sqrt{\frac{GM}{r^3 4\pi^2}}, \quad (4)$$

and relates to the viscous time-scale,

$$\nu_{\rm visc}(r) = \alpha(H/R)^2 \nu_{\rm dyn}(r), \quad (5)$$

where r is the accretion disc radius, H/R and α are the disc scale height and viscosity parameter, respectively, and M is the mass of the central compact object (see e.g. Frank, King & Raine 2002).

For XRBs and AGN the observed broad-band noise variability is generally associated with the viscous time-scales over a range of radii (Arévalo & Uttley 2006; Ingram & Done 2010, 2011). This is motivated by observations of the rms–flux relation seen in many XRBs and AGN (Uttley & McHardy 2001), which imply that the fast variability must be coupled to the slow variability by multiplicative processes (i.e. the resulting variability at the innermost edges of the disc is the product of the variability produced at larger annuli). This can naturally arise as a result of the viscous propagation of material inwards through the disc. The standard model which seeks to reproduce these observations is the fluctuating accretion disc model (Lyubarskii 1997; Kotov, Churazov & Gilfanov 2001), which can correctly reproduce the rms–flux relation as well as the general 1/f shape and high-frequency break observed in most PSDs of XRBs and AGN. In both cases the resulting inner edge of the disc is inferred as being geometrically thick in order to allow the variability to propagate inwards without being damped. On the other hand, some authors have instead associated the break frequency observed in CVs to the dynamical time-scale (equation 4; Revnivtsev et al. 2010, 2012) of the innermost edge of the disc. This association seems to alleviate the problem of a thick disc (since for this interpretation the disc can be either thin or thick), but instead suggests a large disc truncation radius at $\approx 10 R_{\rm WD}$, and evaporation (Meyer & Meyer-Hofmeister 1994) is invoked as a mechanism to deplete the inner disc. Recently the rms–flux relation has also been observed MV Lyrae (Paper I) with the same data as that used in this work, suggesting that the mechanism responsible for mass transfer within the discs, and the associated variability, is similar for CVs, XRBs and AGN, whether this is viscous, dynamical or thermal. The main difference between the rms–flux relation observed in XRBs and that observed in the CV MV Lyrae is the time-scales involved: for XRBs the rms–flux relation is observed in X-rays on time-scales of seconds whilst for MV Lyrae it is observed in optical light on minute time-scales. This time-scale difference can potentially be attributed to the different emitting regions, since the variability observed in X-rays in XRBs is originating deeper within the potential well (thus faster variability) of the accreting compact source when compared to MV Lyrae. The study performed in Paper I concentrated on analysing the high-frequency properties of MV Lyrae, whilst here we concentrate on the broad-band variability properties, and assess whether the observed features are phenomenologically similar to those in XRBs.

Given that the nature of variability is still debated, but recent phenomenological similarities seem to suggest a common origin for CVs, XRBs and AGN, we will, in what follows, associate the characteristic frequencies observed in MV Lyrae to either the viscous or dynamical time-scales, and infer values for the accretion disc structure. This will allow us to compare our results to those inferred from X-ray studies of XRBs and AGN. In the next subsection we will specifically concentrate on the dynamical/viscous interpretations of two Lorentzians, namely L_1 and L_3. The general conclusions drawn from these two components will also hold for the other two Lorentzians as well, and we choose to discuss only L_1 and L_3 as these components seem to display the most interesting trends in Figs 5–7.

4.1 Viscous interpretation

4.1.1 The low-frequency Lorentzian L_3

Here we discuss the possibility that the observed characteristic frequency $\nu_{\rm max,3}$ is associated with the viscous time-scale ($t_{\rm visc}$) at some disc radius. The apparent anticorrelation with flux seen in Fig. 6 could then be suggesting a change in the viscosity parameter α and/or scale height H/R. Observationally, we find that the low-frequency Lorentzian L_3 produces an rms variability of $\approx$5 per cent. As at least that fraction of the luminosity needs to be emitted in the variable emission region, we can first obtain a lower limit on the size of this emitting region.

Measured temperature profiles of CVs with a similar accretion rate seem to follow the theoretical predictions of standard accretion discs up to $\approx 0.05\,{\rm R}_\odot$ (Groot, Rutten & van Paradijs 2001). Closer in, there is some controversy on the shape of the temperature profile, especially for the subclass of CVs SW Sex stars of which MV Lyrae is a member of. Groot, Rutten & van Paradijs (2004) and Groot et al. (2001) have determined a flat-top profile through indirect eclipse mapping, however, Knigge et al. (2000, 2004) have later confirmed the possibility that in the high-luminosity state, at least some SW Sex stars possess a self-occulting component. This could be due to the presence of a thick disc, and would thus result in an observational bias when measuring the temperature profiles in the innermost regions of the accretion disc, producing a flat-top temperature profile.

Because of these controversies we will take the conservative limit and model the minimal size of the emitting region by using the standard disc temperature profile from Frank et al. (2002) (equation 5.49) with a mass accretion rate of $3 \times 10^{-9}\,{\rm M}_\odot\,{\rm yr}^{-1}$ (Linnell et al. 2005). We then summed the emitted blackbody spectra produced at each disc annulus and folded this with the *Kepler* response function,[3] producing the relative cumulative flux emitted by the disc as a function of radius in the top panel of Fig. 9. The figure shows, for example, that if we observe say $\approx$5 per cent rms variability (as observed for L_3), the emitting region must be larger than $\approx 3R_{\rm WD}$. In fact, $3R_{\rm WD}$ in this scenario is a conservative lower limit for two reasons: (i) the absolute amplitude of the variability is larger than $\approx$5 per cent, and (ii) some CVs (namely SW Sex' Groot et al. 2001) show that the disc temperature profile flattens out at larger radii ($\approx 0.2\,{\rm R}_\odot$). Both these effects will push the minimal size of the emitting region to larger radii than those shown in Fig. 9, and further increase the resulting limits on α and H/R.

Having produced an estimate for the minimal size of the variable emitting region, we now place limits on the disc scale height (H/R) and viscosity (α) for the fastest measured time-scales of the Lorentzian L_3 of 0.8 h. This is done as a function of radius in the bottom panel of Fig. 9 (solid lines). The inferred values for α and H/R are too high to be accommodated by the standard thin disc model,

[3] http://keplergo.arc.nasa.gov/CalibrationResponse.shtml

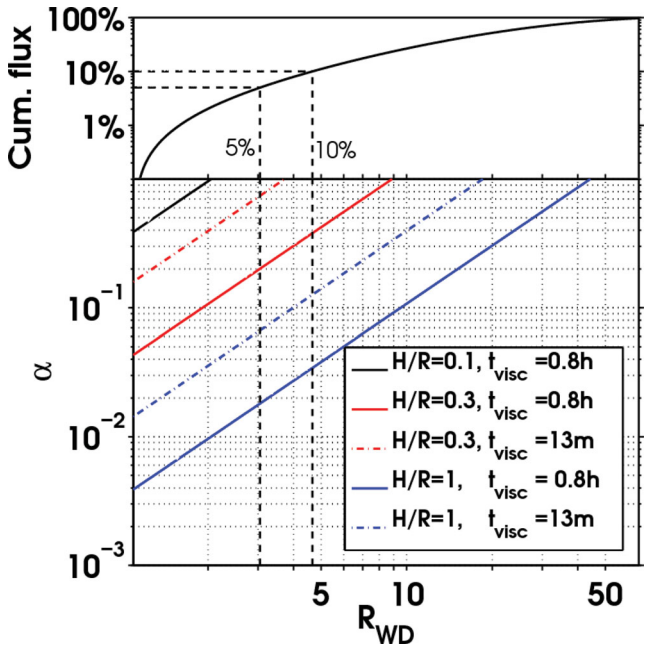

Figure 9. Top: cumulative radial emission profile for the accretion disc in MV Lyrae folded through the *Kepler* passband. Bottom: inferred accretion disc radius and viscosity parameter α for different disc scale heights. The estimates have been obtained by associating the characteristic frequencies of 0.8 h (L_3, solid lines) and 13 min (L_1, dashed lines) to the viscous time-scale at a particular disc radius. The inferred α and H/R values are found to be too large to be accommodated by a standard thin disc. The vertical black dashed lines indicate the minimal extent of the accretion disc given the observed 5 and 10 per cent rms amplitude of the variability.

where $\alpha \leq 0.1$ and $H/R \leq 10^{-2}$ are usually taken. Additionally, the most conservative values for α and H/R (solid black line) are ruled out by the constraints imposed by the minimal size of the emitting region. Thus, if one wants to adopt the viscous interpretation, our result seems to suggest the presence of a geometrically thick accretion disc in order to explain the observed characteristic frequencies of the L_3 Lorentzian. This would be in agreement with the work of Churazov, Gilfanov & Revnivtsev (2001), who have noted that for the fluctuating accretion disc model to work (Lyubarskii 1997; Kotov et al. 2001) and produce the observed rms–flux relation (Arévalo & Uttley 2006; Paper I), one needs a geometrically thick disc.

4.1.2 *The high-frequency Lorentzian L_1*

We find the characteristic frequency of the Lorentzian L_1 to slightly vary throughout the observation, but the data do not allow us to determine whether it correlates with flux. In Paper I (fig. 7) we inferred values of $H/R \approx 0.1$ for $\alpha \approx 1$ assuming the ≈13 min break originates from very close to the WD surface. Here we extend that analysis, and show in Fig. 9 (dashed lines) the dependence on both H/R and α for various disc radii using the inferred PSD break at about 13 min to represent the viscous time-scale. In this case the minimal size of the emitting region is determined by the ≈10 per cent rms variability observed in Fig. 7. Like the situation with the 0.8 h Lorentzian (see Section 4.1.1), this last constraint rules out the most conservative values for α and H/R, suggesting a geometrically thick disc. Furthermore, we note that the constraints inferred from Fig. 9 are likely to be even larger than those inferred here. From the continuum variability modelling of accretion discs performed by Ingram & Done (2010, 2011) we know that the true viscous time-scale at the innermost edge of the disc is even faster than that observed from the PSD break, pushing the inferred α and H/R to even higher values.

One other important result concerning the high-frequency Lorentzian L_1 is the change in fractional rms variability shown in Fig. 7. From the work of Geertsema & Achterberg (1992), we can use the fractional rms as an indication of both α and H/R. This method is based on the effects of magnetohydrodynamic (MHD) turbulence in an accretion disc, and associates the source of flickering to the energy dissipated per unit area at the disc surface. With this method Baptista & Bortoletto (2004) have inferred $\alpha \approx 0.16$ for $H/R = 10^{-2}$ in the CV system V2051 Oph, and comment on this result as being uncomfortably high to be accommodated by the standard thin disc model. In Paper I we also showed how α varies between ≈0.16 and ≈0.62, and invoked an even thicker disc of $H/R \approx 0.1$ to avoid at least the highest α values. The peaks of the rms variability presented in Fig. 7 coincide with a short-duration (few weeks) plateau observed at ≈250 d, and a drop in flux seen at ≈500, both shown in Fig. 1. The behaviour observed in Fig. 7 could be suggesting a change in the geometry and/or viscosity parameter during the observation since the rms variability is tied to both α and H/R in the work of Geertsema & Achterberg (1992). If this were the case however, the inferred range for both α and H/R is quite large ($0.02 < \alpha < 0.2$ and $0.01 < H/R < 0.1$) during the rms change between 5 and 10 per cent, and we caution interpretation of this result as it is not yet clear what physical mechanism is required to explain the observed phenomena.

4.2 Dynamical interpretation

4.2.1 *The low-frequency Lorentzian L_3*

We can alternatively try to associate the obtained characteristic frequencies of the Lorentzian L_3 from Fig. 5 with the Keplerian frequency at a specific disc radius. In order to explain the correlation seen in Fig. 6, the emitting region would then radially grow in size, and increase in temperature, as the time-scale changes from 0.8 to 2.1 h.

Using the highest and lowest frequencies measured for the Lorentzian L_3, we can infer using Kepler's third law an accretion disc size ranging from ≈0.39 $R_\odot$, for the highest frequency, up to ≈0.74 $R_\odot$, for the lowest. These estimates, especially the low-frequency one, are not consistent with the estimated position of the L1 point in this binary system, which sits at about 0.57 $R_\odot$ (Frank et al. 2002). One way to overcome this inconsistency would be to assume that the observed frequency is a beat between the Keplerian outer disc frequency ($\nu_{\rm disc}$) and the orbital frequency ($\nu_{\rm orb}$) of 3.19 h, $\nu_{\rm beat} = \nu_{\rm disc} + \nu_{\rm orb}$. In this case, the outer disc edge would be observed to grow from ≈0.33 to ≈0.53 $R_\odot$, consistent with the disc radially growing in size up to the L1 point. However the other Lorentzians, especially the lowest frequency L_4 Lorentzian, would then require a different mechanism to drive them, as their beat frequency would be too low to be accommodated within the L1 point.

4.2.2 *The high-frequency Lorentzian L_1*

The high-frequency PSD breaks observed in accreting compact objects have also been associated with the Keplerian time-scale at the innermost edge of accretion discs. Specifically, Revnivtsev et al. (2012, 2010) have associated the PSD breaks observed in some magnetized WDs, NSs and the well-known CV SS Cyg to

the dynamical time-scale at the innermost edge of the accretion disc. They inferred relatively large inner disc truncation radii for all systems they studied, and for SS Cyg in particular they inferred a truncation radius of $\approx 10 R_{\rm WD}$. In order to deplete the inner disc Revnivtsev et al. (2010) suggest evaporation (Meyer & Meyer-Hofmeister 1994) as a mechanism to truncate the thin disc away from the WD surface.

The break frequency observed in SS Cyg is very similar to the one observed here in MV Lyrae, and it is possible that we also observe the Keplerian frequency at the innermost edge of the accretion disc truncated at about $\approx 10 R_{\rm WD}$. We note, however, that dynamical processes will be more easily damped, as compared to viscous process, whilst they propagate through disc. This is because viscous damping will suppress the fast dynamical variability but not the slower viscous variability. As a result dynamical effects are observed as additive process in light curves, whilst viscous ones as multiplicative. The presence of the rms–flux relation at high frequencies thus suggests viscous interactions as the main source of variability, since additive processes would destroy the observed rms–flux relation.

5 CONCLUSION

We have presented an analysis of the broad-band frequency behaviour of the accreting WD MV Lyrae based on data obtained by the *Kepler* satellite. We have shown how the complex PSD can be decomposed with a number of Lorentzian-shaped functions. We further searched for possible correlations between the characteristic frequencies, and found the first frequency varying QPO in a CV, where frequency is inversely proportional to mean source flux.

The characteristic frequencies associated with the fitted Lorentzians were used to explore the origin of variable emission in terms of viscous or dynamical processes as the two limiting cases. In the former case we infer extremely high values of both disc scale height $H/R \geq 0.3$ and viscosity $\alpha \geq 0.1$, suggesting the existence a geometrically thick disc. This result is potentially in line with the work of Knigge et al. (2000, 2004), which have suggested the presence of a self-occulting accretion disc close to the WD. In the dynamical case we instead infer a large disc truncation radius of $\approx 10 R_{\rm WD}$, but the presence of other components undermines a dynamical interpretation, at least for the lowest frequency components. More importantly, the presence of the rms–flux relation observed in MV Lyrae (Paper I) and other XRBs/AGN (Uttley & McHardy 2001), potentially rule out dynamical effects as the source of variability (since the fast dynamical variability will be damped), but favours a viscous origin for the observed broad-band noise components, at least at the highest observed frequencies.

In summary both viscous and dynamical (and consequently thermal) time-scales struggle to consistently explain the observed broad-band variability in MV Lyrae. However, our analysis seems to suggest, at least phenomenologically, that the mechanisms which give rise to the observed rms–flux relation(s) and characteristic frequencies observed here and in other XRBs/AGN need to occur in all accretion discs (whether they are thin or thick), possibly suggesting a similar physical origin for the variability in both types of systems.

The broad-band variability properties of MV Lyrae remain yet to be fully understood. More generally, the variability properties of both CVs and XRBs also remain an enigmatic observational feature. Although both types of systems possess an accretion disc which is in many ways similar, there has not yet been enough observational data to provide a complete comparative study of the broad-band variability properties. However, it is clear that the phenomenological properties between the broad-band variability observed in MV Lyrae and in XRBs and AGN are very similar (when appropriately scaled), and are potentially driven by a common accretion mechanism.

ACKNOWLEDGMENTS

This paper includes data collected by the *Kepler* mission. Funding for the *Kepler* mission is provided by the NASA Science Mission directorate. This research has made use of NASA's Astrophysics Data System Bibliographic Services. SS acknowledges funding from NWO project 600.065.140.08N306 to PJG. MS acknowledges funding from the NASA grant NNX11AB86G. SS wishes to acknowledge G. Nelemans and A. Achterberg for useful and insightful discussions.

REFERENCES

Arévalo P., Uttley P., 2006, MNRAS, 367, 801
Baptista R., Bortoletto A., 2004, AJ, 128, 411
Belloni T., Psaltis D., van der Klis M., 2002, ApJ, 572, 392
Churazov E., Gilfanov M., Revnivtsev M., 2001, MNRAS, 321, 759
Frank J., King A., Raine D. J., 2002, Accretion Power in Astrophysics, 3rd edn. Cambridge Univ. Press, Cambridge
Geertsema G. T., Achterberg A., 1992, A&A, 255, 427
Gilliland R. L. et al., 2010, ApJ, 713, L160
Groot P. J., Rutten R. G. M., van Paradijs J., 2001, A&A, 368, 183
Groot P. J., Rutten R. G. M., van Paradijs J., 2004, A&A, 417, 283
Hoard D. W., Linnell A. P., Szkody P., Fried R. E., Sion E. M., Hubeny I., Wolfe M. A., 2004, ApJ, 604, 346
Ingram A., Done C., 2010, MNRAS, 405, 2447
Ingram A., Done C., 2011, MNRAS, 415, 2323
Jenkins J. M. et al., 2010, ApJ, 713, L87
Knigge C., Long K. S., Hoard D. W., Szkody P., Dhillon V. S., 2000, ApJ, 539, L49
Knigge C., Araujo-Betancor S., Gansicke B. T., Long K. S., Szkody P., Hoard D. W., Hynes R. I., Dhillon V. S., 2004, ApJ, 615, L129
Kotov O., Churazov E., Gilfanov M., 2001, MNRAS, 327, 799
Linnell A. P., Szkody P., Gansicke B., Long K. S., Sion E. M., Hoard D. W., Hubeny I., 2005, ApJ, 624, 923
Livio M., Pringle J. E., 1994, ApJ, 427, 956
Lubow S. H., 1991, ApJ, 381, 259
Lyubarskii Y. E., 1997, MNRAS, 292, 679
Mauche C. W., 2002, ApJ, 580, 423
Meyer F., Meyer-Hofmeister E., 1994, A&A, 288, 175
Miyamoto S., Kimura K., Kitamoto S., Dotani T., Ebisawa K., 1991, ApJ, 383, 784
Montgomery M. M., 2012, ApJ, 745, L25
O'Donoghue D., Charles P. A., 1996, MNRAS, 282, 191
Osaki Y., 1989, PASJ, 41, 1005
Pretorius M. L., Warner B., Woudt P. A., 2006, MNRAS, 368, 361
Revnivtsev M. et al., 2010, A&A, 513, A63
Revnivtsev M. G., Burenin R. A., Tkachenko A. Y., Khamitov I. M., Ak T., Merloni A., Pavlinsky M. N., Sunyaev R. A., 2012, Astron. Lett., 38, 238
Scaringi S. et al., 2010, MNRAS, 401, 2207
Scaringi S., Körding E., Uttley P., Knigge C., Groot P. J., Still M., 2012, MNRAS, 421, 2854 (Paper I)
Shakura N. I., Sunyaev R. A., 1973, A&A, 24, 337
Skillman D. R., Patterson J., Thorstensen J. R., 1995, PASP, 107, 545
Summons D. P., Arévalo P., McHardy I. M., Uttley P., Bhaskar A., 2007, MNRAS, 378, 649
Uttley P., McHardy I. M., 2001, MNRAS, 323, L26
Warner B., 2004, PASP, 116, 115
Whitehurst R., 1988, MNRAS, 232, 35
Wood M. A., Still M. D., Howell S. B., Cannizzo J. K., Smale A. P., 2011, ApJ, 741, 105

This paper has been typeset from a TEX/LATEX file prepared by the author.